UDC 621.9.047.666.792

B. Staniewicz-Brudnik (Kraków, Poland)
S. Szarska (Wroclaw, Poland)
K. Gamrat (Kraków, Poland)

The influence of mechanochemical treatment of sintered submicrocrystalline corundum substrates on the structure of bioglass composites

The influence of mechanochemical treatment of submicrocrystalline sintered corundum on the structure of bioglass composites containing α-Al_2O_3 and $CaO—SiO_2—P_2O_5$ glasses was examined in the context of the possibility to form hydroxyapatite after being immersed in the simulated body fluid solution. Measurements of specific surface area and size and X-ray analysis of submicrocrystalline sintered corundum were conducted. Bioglass composites were obtained by placing submicrocrystalline sintered corundum grains in the $CaO—SiO_2—P_2O_5$ sol system, gelling and sintering at 800 °C. The specimens were examined under a scanning electron microscope before and after immersion in the simulated body fluid solution for 24 and 120 h. Using the VCS algorithm, calculations of thermodynamic stability of compounds occurring in these bioglass composites were carried out, verifying the X-ray analysis.

Key words: *mechanochemical treatment, submicrocrystalline sintered corundum, bioglass composite, hydroxyapatite, SBF, SEM, VCS algorithm.*

Introduction. Current medicine makes use of numerous synthetic reconstructed biomaterials ranging from simple tissue replacements to complicated prostheses [1, 2]. Biomaterials can be grouped according to:

— chemical composition (metallic, polymer, ceramic, composite);

— microstructure (dense, macroporous, microporous);

— biocompatibility (biocompatible materials — some metals, resorbable polymers and bioactive materials, inert ceramics; materials with limited biocompatibility — the majority of metals, alloys, polymers; toxic materials).

On account of the numerous advantages (biocompatibility, a high hardness, a low wear) ceramic biocomposites play an important role in designing and producing implants and in tissue engineering as medication media. From the beginning of the seventies, experimental and clinical examinations regarding tissue reactions to composite corundum materials have been conducted. Hulbert et al., investigating porous materials, described the sequence of load transfers after corundum implantation in bone tissue [3]. They were trying to answer the question of whether the surrounding tissue is permeable to aluminum. Arentowicz et al. [4] used absorption atomic spectroscopy to measure the content of different elements in the bone surrounding the implant and did not detect aluminum. This is contradictory to the conclusions of Lewandowska-Szumieł [5], who reported the presence of Al in the tissue adjacent to the corundum implant. Ogushi et al. [6], when examining the osteogenic activity of human bone marrow cells on the surface of corundum ceramics in vitro, demonstrated that cells of the bone marrow diversify toward bone

cells (osteoblasts), which leads to mineralization of the bone tissue. Barrere observed and interpreted changes on the surface of corundum and TiO_2 after immersion in the simulated body fluid solution (SBF) [7]. There is little information on an electric charge which arises on surface layers of glassy biocomposites as a result of reaction with the tissue fluid and electromagnetic radiation. Szarska et al. [8—10] examined the influence of external factors (deformation, ionizing radiation, low temperatures) on surface transport processes in bioglassy composites. Ślósarczyk et al. [11] examined the effect of addition of calcium and magnesium phosphates as microstructure modifiers of bioactive multifunctional ceramic materials. The influence of CaO and MgO on physico-mechanical properties of the corundum biomaterials was studied by Jaegermann et al. [12, 13].

The glasses of the CaO— SiO_2—P_2O_5 are characterized by a much higher biological activity compared to metals, carbon and oxides, such as corundum, which, being biologically inert, in turn is far more biocompatible. These glasses have both appropriate chemical composition and surface activity to enable the physiological environment to react selectively with some of their constituents to combine the surface with live tissue.

Below the effect of mechanochemical treatment (high-energy milling) of sintered submicrocrystalline corundum on the microstructure of a biocomposite formed is discussed.

Experimental Procedures

Input materials. *Submicrocrystalline sintered corundum*. Submicrocrystalline sintered corundum grains were supplied by the 3M Company.

This material is sintered α-Al_2O_3 having an ultradispersed structure obtained by transforming the sol into the magnesia-modified gel. This results in a specific structure of short Al_2O_3 needles separated by microthreads of $MgAl_2O_4$. The material properties were as follows [14]:

— density — 3.9317 g/cm^3;
— microhardness — 17—21 GPa;
— compressive strength — 22 MPa;
— fracture toughness — approx. 4 MPa·m$^{1/2}$;
— Young's modulus — 362 GPa.

The corundum grains of the input granulation were milled for 5, 10, and 15 h in a Fritsch Pulverisette 6 planetary ball mill in ethanol using agate balls. The total mass of the submicrocrystalline sintered corundum grains was 50 g and the ball to powder ratio was 10:1. This mechanochemical treatment (high-energy milling) increases the material specific surface area, changes the material structure, generating dislocations and point defects, which favor microarea reactivity. A small quantity of powder was taken from the mill chamber after milling during 5, 10, and 15 h to make analyses.

Measurements of specific surface area were made with a Micrometric ASAP 2010 apparatus using the physical adsorption of nitrogen method at 77 K. Analysis of the size composition was made in Micromeritics Sedigraph 5.100 X-ray Analyzer using 0.5 % sodium pyrophosphate solution as a sedimentation liquid. X-ray examination of cubitron after milling was conducted in a Philips diffractometer with a cobalt source in 2θ range of 10—90°. SEM examinations of the milled submicrocrystalline sintered corundum as well as of the bioglass composites were carried out under a Jeol 64 LV scanning microscope in a low vacuum.

The CaO—SiO_2—P_2O_5 glass system, the gel. The chemical composition of the glass system is given in Table 1.

Table 1. Glass composition, mol%

SiO_2	CaO	P_2O_5
58	33	9

To prepare the solutions for immersion of corundum grains, the following constituents were employed:

— tetraethoxysilane (TEOS) $Si(OC_2H_5)_4$;

— triethyl phosphite (TEP) OP $(C_2H_5)_3$;

— calcium nitrate tetrahydrate $Ca(NO_3)_2*4H_2O$;

— water (H_2O) as a catalyst of hydrolysis.

The order in which the chemicals were added and times of mixing [2, 3] are shown in Fig. 1. The basic composition of hydrolysate with the addition of $Ca(NO_3)_2*4H_2O$ and OP $(C_2H_5)_3$ was stirred with a magnetic stirrer.

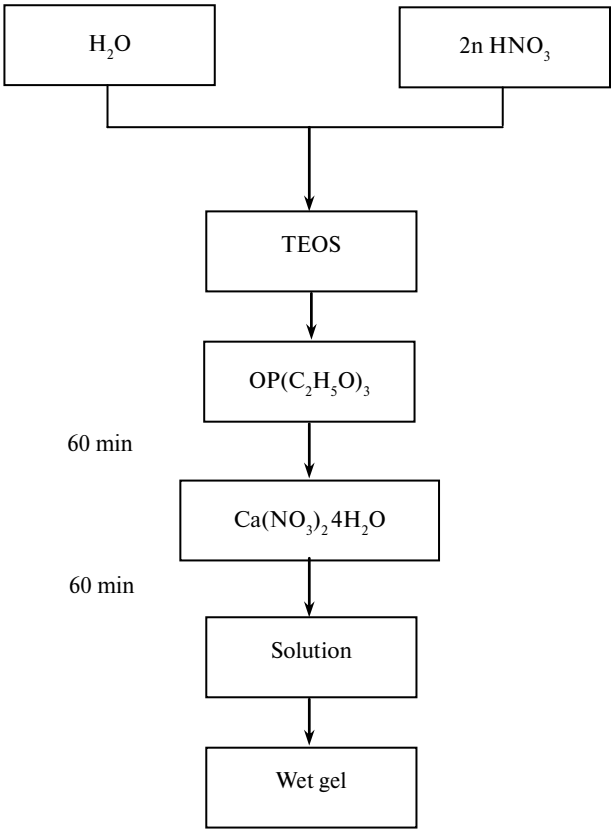

Fig. 1. The scheme of preparing input materials for bioglass composite syntesis by Jones.

Simulated body fluid. SBF is a synthetically produced physiologic saline solution imitating natural plasma, in which a balance is maintained between concentration of H^+ and OH^- ions, with the pH being approximately 7.3 (Table 2) [5]. Action of the SBF solution on bioactive gel leads to the formation of hydroxyapatite, which facilitates the formation of a permanent bond with the bone.

Table 2. Ion concentration, mM, in the human body blood plasma (NBF) and simulated body fluid (SBF)

	Na^+	K^+	Ca^+	Mg^{2+}	Cl^-	HCO_3^-	HPO_4^-	SO_4^{2-}
NBF	142.0	5.0	2.5	1.5	103.0	27.0	1.0	0.5
SBF	142.0	5.0	2.5	1.5	147.0	4.2	1.0	0.5

The biocomposite. As-received and milled corundum grains were added to the hydrolysate in the ratio 1 : 0.028 and left under ambient conditions to be gelled, which occurred after 7 to 14 days depending on the quantity of water used. The gels were heater-dried at 60 °C for three days and then heated in an electric furnace at 800 °C for 2 h. During the heat treatment the remaining water (in the form of steam [4]) and gaseous organic compounds (principally CO_2) were removed. Closure of xerogel pores also occurred. Biocomposite samples were immersed in SBF at 37 °C, held there for 24 and 120 h, and then examined under the scanning electron microscope. Thermodynamic calculations of the phase equilibria were based on the VCS algorithm.

Results and discussion. The specific surface area (S_{BET}) of submicrocrystalline sintered corundum grains grew by a factor of two, from 5.17 to 10.95 m^2/g, as a result of the mechanochemical treatment (Table 3, Fig. 2). This effect is illustrated

Table 3. Results of size analysis and specific surface area of submicrocrystalline sintered corundum after milling

Fraction	Milling time, h		
	15	10	5
Below 20 μm	100.0	100.0	100.0
15 μm	99.6	100.0	95.1
10 μm	97.1	97.2	81.3
8 μm	94.9	94.1	71.5
6 μm	91.1	87.2	59.7
5 μm	87.1	81.1	52.7
4 μm	80.2	72.0	44.4
3 μm	69.0	59.5	35.2
2 μm	53.0	44.5	26.1
1.5 μm	43.9	36.2	21.4
1.0 μm	33.1	26.8	15.7
0.8 μm	27.8	22.1	12.8
0.6 μm	20.9	16.6	9.5
0.5 μm	16.4	13.4	7.6
0.4 μm	11.2	9.8	5.7
0.3 μm	4.8	5.6	3.1
Median, μm	1.83	2.35	4.66
Mode, μm	2.82	3.61	8.68
Grain surface area, m^2/g (by Stoke's)	1.509	1. 286	0.870
Specific surface area S_{BET}, m^2/g	10.95	8.74	5.17

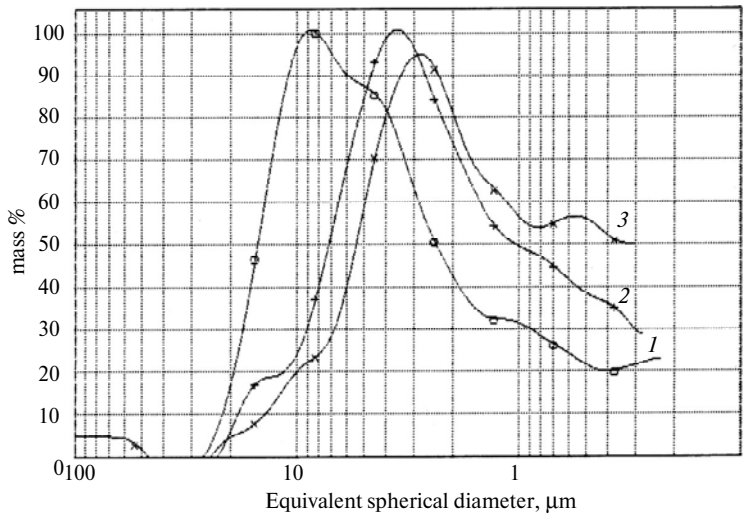

Fig. 2. The effect of the milling time (5 (*1*), 10(*2*), 15 (*3*) h) on the grain size reduction–population curves.

in the size distribution plots (population curves): multimodal, curves *1* (5-hour milling) and *3* (15-hour milling), and monomodal, curve *2* (10-hour milling), and of mode and median values. After 5-hour milling the three dominant populations were: below 0.5, between 0.5 and 1.5, and between 1.5 and 20 μm. After 10 h the dominant population was between 0.3 and 10 μm, and after 15-hours milling, there were two dominant populations: 0.3—1 and 1—15 μm, respectively. The largest effect of milling was observed after 10 h, since after 15-hour milling agglomeration of the smallest grains was evident.

X-ray radiography of the input material revealed the presence of alpha, gamma, and kappa phases of Al_2O_3, $Al_{12}Mg_{17}$ and $MgAl_2O_4$. Additionally, quartz (SiO_2) appeared during milling, originating from agate balls. The polymorphic changes from α-Al_2O_3 to κ-Al_2O_3 as a result of mechanochemical treatment were observed.

Calculations of crystal sizes according to the Scherer equation showed reduction of sizes (Table 4) from 128.9 to 71.7 nm, which was also confirmed by scanning electron microscopy (Figs. 3, 4). Samples of bioglass composites (after gelling and heat treatment) exhibited a macroscopically visible gradient structure (Fig. 5). For composites with unmilled grains, two layers were clearly visible: a lower layer, which was blue and contained grains of the submicrocrystalline sintered corundum, and an upper layer, which was white and constituted the bioglass (Figs. 6, 7).

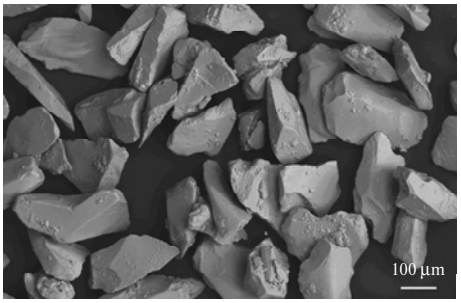

Fig. 3. SEM image of submicrocrystalline sintered corundum, 100×.

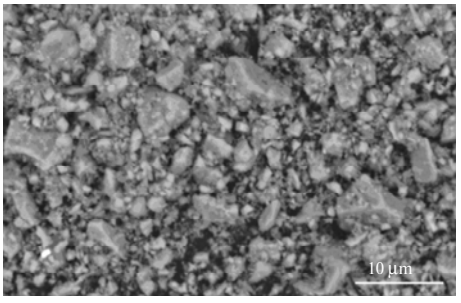

Fig. 4. SEM image of submicrocrystalline sintered corundum after 15-hour milling, 2500×.

Table 4. X-ray identification of α-Al_2O_3 before and after milling

Before milling	Milling time, h		
	5	10	15
Al_2O_3 (corundum)	Al_2O_3 (corundum)	Al_2O_3 (corundum)	Al_2O_3 (corundum)
γ-Al_2O_3	γ-Al_2O_3	γ-Al_2O_3	γ-Al_2O_3
Θ-Al_2O_3	Θ-Al_2O_3	Θ-Al_2O_3	Θ-Al_2O_3
	κ-Al_2O_3	κ-Al_2O_3	κ-Al_2O_3
$Al_{12}Mg_{17}$	$Al_{12}Mg_{17}$	$Al_{12}Mg_{17}$	$Al_{12}Mg_{17}$
$MgAl_2O_4$	$MgAl_2O_4$	$MgAl_2O_4$	$MgAl_2O_4$
	SiO_2 (quartz)	SiO_2 (quartz)	SiO_2 (quartz)
	Crystal size of α-Al_2O_3, nm		
138.3	128.9	85.9	71.7

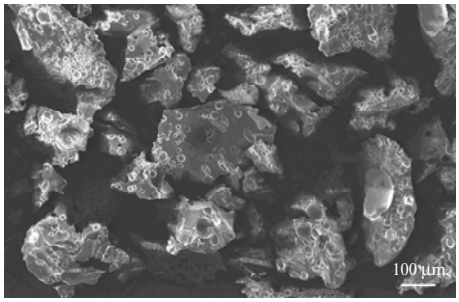

Fig. 5. SEM image of the CaO—SiO_2—P_2O_5 bioglass.

Fig. 6. Photograph of the bioglass composite with the unmilled submicrocrystalline sintered corundum.

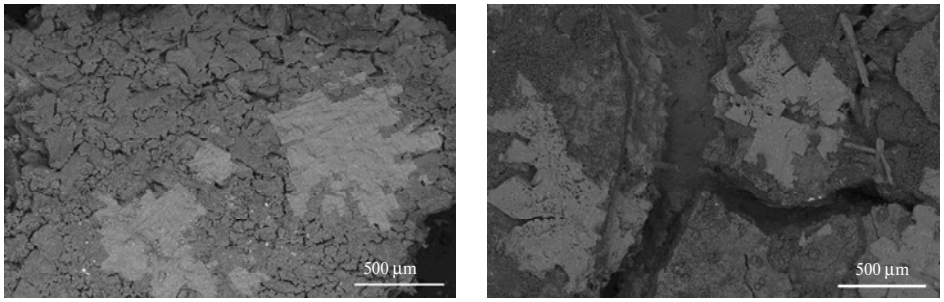

a *b*

Fig. 7. SEM image of the bioglass composite with the submicrocrystalline sintered corundum (unmilled), a top (*a*) and a pit (*b*) of the sample.

Scanning electron microscopy showed that the finer the submicrocrystalline corundum, the more uniform was the composite (Figs. 8, 9). A biocomposite sample of unmilled grains in the lower part (defined as the surface) contained principally Al, O and traces of Ca, P and Si. In the upper layer calcium, phosphorous, silicon, traces of aluminum and carbon, which confirmed the possibility of forming calcites were visible. The "upper side" of all the composites showed the clearly defined crackins, the main reason for which was an increase in the capillary pressure of the liquid in gel pores and an increase in the surface tension of the liquid—steam system. As the capillary pressure gradient developed in the sample volume due to the

limited transport of liquid accumulated in pores, the unequal stress distribution resulted in cracking the material.

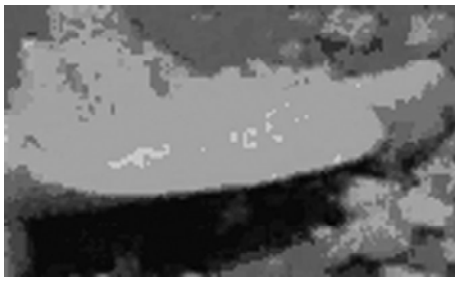

Fig. 8. Photograph of the bioglass composite with the submicrocrystalline sintered corundum after 10-hour milling.

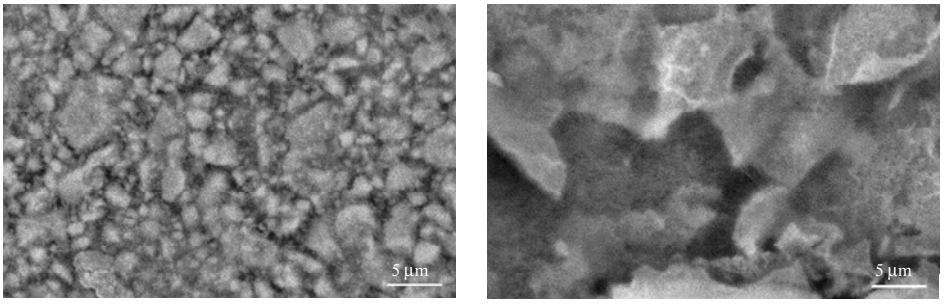

a *b*

Fig. 9. SEM image of the bioglass composite with the submicrocrystalline sintered corundum (after 10-hour milling), a pit (*a*) and a top (*b*) of the sample.

So that crystallization of hydroxyapatite could occur on the biocomposite surface, certain conditions had to be satisfied:

— the solution in direct contact with the biocomposite surface should be saturated with calcium ions in relation to hydroxyapatite; in the case of glass, the source of calcium ions was the glass phase;

— surface charge should be negative, silica gel, which forms on the biocomposite surface, possesses such a charge;

— in the surface layer there should be areas favorable for nucleation of hydroxyapatite; hydroxyl groups are such places;

— crystallization of hydroxyapatite on the material surface is only possible when Si—OH groups are present in the surface layer. This in turn is possible when the heat treatment temperature does not exceed 900 °C;

— crystallization of hydroxyapatite, which favors maintenance of sterile conditions in the process of making the samples.

Various combinations of calcium and phosphorus oxides provide a large variety of calcium phosphates, which can be classified according to the type of the phosphate anion: ortho-(PO_4^{3-}), meta-(PO_3^-), pyro-($P_2O_7^{4-}$), and poly-$(PO_3)_n^{n-}$. In the $Ca(OH)_2$—H_3PO_4—H_2O ternary system [8] there are eleven known non-ion-substituted calcium orthophosphates with the Ca/P molar ratio within 0.5—2.0. Molar ratios indicate: 1.0 — dicalcium phosphate dehydrate; 1.2—2.2 — amorphous calcium phosphate; 1.5—1.67 — calcium deficient hydroxyapatite, and 1.67 — hydroxyapatite [15].

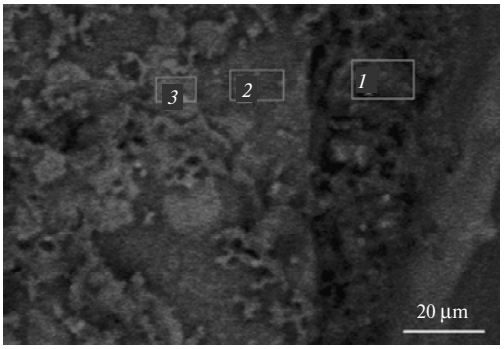

a

Image4-1

Elt.	Line	Intensity (c/s)	Error 2-sig	Conc	
C	Ka	0.00	0.000	0.000	wt.%
O	Ka	0.82	0.332	30.175	wt.%
Na	Ka	2.96	0.628	15.249	wt.%
Mg	Ka	0.19	0.159	0.826	wt.%
Al	Ka	0.54	0.269	1.916	wt.%
Si	Ka	1.58	0.459	4.719	wt.%
P	Ka	0.98	0.361	3.019	wt.%
Cl	Ka	7.53	1.002	22.837	wt.%
Ca	Ka	6.07	0.900	21.259	wt.%
				100.000	wt.% Total

Image4-2

Elt.	Line	Intensity (c/s)	Error 2-sig	Conc	
C	Ka	3.43	0.677	31.209	wt.%
O	Ka	7.51	1.000	32.203	wt.%
Na	Ka	1.18	0.396	0.725	wt.%
Mg	Ka	0.07	0.098	0.030	wt.%
Al	Ka	0.21	0.166	0.072	wt.%
Si	Ka	43.88	2.419	13.264	wt.%
P	Ka	19.86	1.627	7.336	wt.%
Cl	Ka	14.29	1.380	5.355	wt.%
Ca	Ka	24.80	1.818	9.806	wt.%
				100.000	wt.% Total

B+C0 wnetrze analiza w obszarach 1000...

Elt.	Line	Intensity (c/s)	Error 2-sig	Conc	
C	Ka	2.31	0.555	21.259	wt.%
O	Ka	7.47	0.998	37.295	wt.%
Na	Ka	1.02	0.368	0.756	wt.%
Mg	Ka	0.19	0.161	0.096	wt.%
Al	Ka	0.54	0.268	0.219	wt.%
Si	Ka	13.78	1.355	4.784	wt.%
P	Ka	31.70	2.056	11.986	wt.%
Cl	Ka	12.71	1.301	5.211	wt.%
Ca	Ka	42.10	2.369	18.394	wt.%
				100.000	wt.% Total

b

Fig. 10. SEM image of the bioglass composite with the unmilled submicrocrystalline sintered corundum, five days in the SBF solution, 1000×.

SEM observations demonstrated that a 24-hour immersion in SBF resulted in the formation of calcites and various types of calcium phosphate (Ca/P molar ratio ≤ 1). After a 5-day immersion, on the surfaces of biocomposites containing unmilled and milled for 10 h cubitron grains, hydroxyapatite appeared, as was evidenced by the Ca/P molar ratio of 1.5—1.7 in selected points (Fig. 10) In the remaining samples, most probably, calcium phosphate crystallized on the biocomposite surface.

The chemical stability of bonds between submicrocrystalline sintered corundum and components of the $CaO—SiO_2—P_2O_5$ glass system was examined by calculating the thermodynamic potential by the VCS algorithm method which considers the stability of all reaction products [16]. Calculation of equilibrium was conducted for glass composites at 310 K (37 °C) at atmospheric pressure. Molar ratios of components were adopted as their actual values. The method used was of minimization of the thermodynamic potential of the whole mixture. Such calculations do not require specifying the reactions and their number, through which the system reaches equilibrium; it only requires specifying the substances, which could exist in the reaction, but did not. Out of 46 possible reaction products, only Al_2O_3, Al_2SiO_5, $Ca_3(PO_4)_2$ and $CaAl_2Si_2O_8$ turned out to be thermodynamically stable. The presence of them was confirmed by X-ray analysis (Table 4).

Conclusions

Based on the investigation carried out so far the following can be concluded:

The degree of size reduction of submicrocrystalline sintered corundum has a significant influence on the uniformity of bioglass composites.

Mechanochemical treatment (high-energy milling) for 5, 10 and 15 hours changed the chemical composition of submicrocrystalline sintered corundum. Some of α-Al_2O_3 grains after 10-hour milling are transformed to kappa Al_2O_3 (from

1 to 6 vol%). Further milling did not change the submicrocrystalline sintered corundum.

Gradient bioglass composites can be produced by immersing corundum grains in the sol of $CaO—SiO_2—P_2O_5$ glass system, gelling and sintering at 800 °C. But the finer the submicrocrystalline sintered corundum grains, the more homogenous the composite.

Calculations of the thermodynamic stability of bioglass composites based on the VCS algorithm showed that only four compounds (Al_2O_3, Al_2SiO_5, $Ca_3(PO_4)_2$, $CaAl_2Si_2O_8$) out of 46 possibilities were stable. The presence of them was confirmed by the X-ray analysis.

Immersion of samples of bioglass composites in the SBF solution for 24 h caused the appearance of calcites. After immersing the samples in the SBF solution for 5 days hydroxyapatite appeared on composite samples of two types. Those were unmilled grains of submicrocrystalline sintered corundum and samples milled for 10 h. The latter were of Ca/P molar ratios of 1.5, 1.7, 1.6, 1.7 at different points on the surface.

1. *Hench L. L.* Biomaterials: a forecast for the future // Biomaterials. — 1998. — **19**. — P. 1419—1423.
2. *Jaegermann Z.* Porowata bioceramika korundowa. — Doctor's thesis AGH. — Crakow, 2005.
3. *Hulbert S. F., Cooke F. W., Klawitter J. J. et al.* Attachment of prostheses to the musculosceletal system tissue ingrowth and mechanical interlocking // J. Biomed. Mater. Res. Symp. — 1973. — **4**. — P. 1—23.
4. *Arentowicz G. and co-workers.* Zawartość pierwiastków w kości wokół wszczepu ceramicznego Al_2O_3 // Prot. Stom. — 1992. — **6**. — P. 228—232.
5. *Lewandowska-Szumieł M., Komender J.* Aluminium release as a new factor in the estimation of alumina bioceramic implants // Clinical Materials. — 1990. — **5**. — P. 167—175.
6. Takaoka T., Okumura M., Ohgushi H. et al. Osteogenic activity of human marrow cells on alumina ceramics // Biomaterials. — 1996. — **17**, N 15. — P.1499—1505.
7. *Barrere and co-workers* // Calcium phosphate interactions with titanium oxide and alumina substrates: an XPS study // J. Mater. Sci. Mat. Med. — 2003. — **14**. — P. 419—425.
8. *Szarska S., Jungner H., Borsowska A.* Influence of ionizing radiation on biogel bone implants observed by luminescence measurements // Radiat. Meas. — 2004. — **38**. — P. 497—500.
9. *Szarska S., Niemczyk S.* Surface charge induced on bioactive composite // Inżynieria Biomateriałów. — 2006. — **58**—**60**. — P. 248—250.
10. *Szarska S.* Pomiar ładunku powierzchniowego w modyfikowanych szkłach biologicznie czynnych // Ceramika. — 1994. — **46**. — P. 303—306.
11. *Ślósarczyk A., Rapacz-Kmita A.* Bioaktywne ceramiczne materiały kompozytowe // Ceramika Materiały Ogniotrwałe. — 2004. — **56**, N 4. — P. 144—149.
12. *Jaegermann Z., Rapacz-Kmita A., Ślósarczyk A., Chrościcka A., Lewandowska-Szumieł M.* Wpływ domieszek CaO i MgO na właściwośći biotworzywa korundowego, part III // Szkło i Ceramika. — 2005. — **56**, N 6. — P. 12—16.
13. *Jaegermann Z., Michałowski S., Karaś J., Chrościcka A., Lewandowska-Szumieł M.* Porowate nośniki korundowe do zastosowania w inżynierni tkankowej // Ibid. — 2006. — **57**, N 4. — P. 16—20.
14. *Staniewicz-Brudnik B., Procyk B. Środa M., Majewska-Albin* K. Special glasses with submicrocrystalline sintered alumina admixture in cBN tools // Optica Applicata. — 2003. — **XXXIII**, N 1. — P. 167—174.
15. *Dorozkhin S. V.* Calcium ortophosphates // J. Mater. Science. — 2007. — **42**. — P. 1061—1095.
16. *Benko E., Wyczesany A.* Calculation of chemical equilibria in the Mo—B—N system // J. Eur. Ceramic Society. — 1994. — **14**. — P. 557—562.

Institute of Advanced Manufacturing Technology
Institute of Physics, Wroclaw University of Technology
Institute of Chemistry, Kraców University of Technology

Received 11.04.08